



Research Article

## Biomechanical Simulation and Comparison of Scepter Plate and PHILOS Systems for Greater Tuberosity Humerus Fracture Fixation

Ratthapoom Watcharopas

Medical Engineering Program, Faculty of Engineering, Thammasat University, Pathum Thani, Thailand  
Thammasat University Center of Excellence in Computational Mechanics and Medical Engineering, Thammasat University, Pathum Thani, Thailand  
Vejthani Hospital, Bangkok, Thailand

Phongsiri Kansue

Department of Mechanical Engineering, Faculty of Engineering, Thammasat University, Pathum Thani, Thailand  
Thammasat University Center of Excellence in Computational Mechanics and Medical Engineering, Thammasat University, Pathum Thani, Thailand

Wiroj Limtrakarn\*

Medical Engineering Program, Faculty of Engineering, Thammasat University, Pathum Thani, Thailand  
Department of Mechanical Engineering, Faculty of Engineering, Thammasat University, Pathum Thani, Thailand  
Thammasat University Center of Excellence in Computational Mechanics and Medical Engineering, Thammasat University, Pathum Thani, Thailand

\* Corresponding author. E-mail: limwiroj@engr.tu.ac.th DOI: 10.14416/j.asep.2025.03.005

Received: 24 August 2024; Revised: 10 November 2024; Accepted: 31 January 2025; Published online: 19 March 2025  
© 2025 King Mongkut's University of Technology North Bangkok. All Rights Reserved.

### Abstract

This paper presents a biomechanical study of a proximal humerus locking plate (PHILOS) and a new locking plate for the humerus fracture treatment of greater tuberosity. A new locking plate is designed in a scepter shape. Fiber wire is applied to reduce the number of screws. The finite element model was conducted to evaluate the biomechanical behavior of the scepter locking plate-screw-wire fixation under natural loading conditions, i.e., contraction force 200 N and 100 N on supraspinatus and infraspinatus tendons, respectively, and compared to the PHILOS plate-screw-wire fixation. The model consists of cortical bones of the humerus, supraspinatus and infraspinatus tendons, both locking plates, screws, and fiber wires. The maximum von Mises stress and factor of safety on the PHILOS plate and scepter locking plate are 334.1 N/mm<sup>2</sup>, 2.07, and 590.9 N/mm<sup>2</sup>, 1.17, respectively. The maximum strain of two crack surfaces and maximum displacement of fracture gap of the PHILOS system model and scepter locking plate system model were 0.3937%, 0.54 mm, and 0.492%, 0.49 mm, respectively. The proper strain and maximum displacement of fracture gap that can promote primary healing are less than 2% and 1 mm, respectively. The results indicate that the scepter locking plate-screw-wire fixation exhibits comparable or non-inferior biomechanical behavior and no effect on the healing process, including stiffness and stress concentration, but 21% smaller, 45% shorter, and 74% lower volume and weight than the PHILOS plate-screw-wire fixation. The scepter locking plate also obtains smaller incisions and reduces soft tissue trauma. These findings suggest that the scepter locking plate design, including screw-wire fixation, is more specifically tailored to the humerus fracture treatment of greater tuberosity than PHILOS plate-screw-wire fixation and may offer advantages in surgical technique and outcome. This scepter locking plate system could be a viable alternative for the fracture treatment of greater tuberosity.

**Keywords:** Biomechanical comparison, Fiber wire, Finite element analysis, Greater tuberosity, Humerus fracture, PHILOS plate, Scepter locking plate

## 1 Introduction

The humeral fractures of Greater tuberosity (GT) represent frequent injuries, comprising roughly 15% of all humeral fractures [1]. Managing these fractures poses a considerable challenge due to the potential for substantial morbidity and functional limitations if not addressed correctly. The conventional treatment modalities for greater tuberosity fractures encompass conservative strategies involving immobilization and physical therapy, open reduction and internal fixation (ORIF), or arthroplasty [2]. Nevertheless, determining the most advantageous treatment methodology remains a matter of contention, emphasizing the necessity for new implant designs to enhance surgical results.

Locking plates have gained popularity as a treatment option for humeral fractures, including those involving greater tuberosity. Among these implants, the proximal humeral internal locking system (PHILOS) is frequently employed for its demonstrated ability to provide stable fixation and favorable clinical results [3]–[5]. Notably, it offers superior fixation strength compared to screws, double-row transosseous sutures, and tension band techniques [6].

Suture augmentation attaching the rotator cuff to the PHILOS plate has been recommended to counter the traction force of the rotator cuff on tuberosity, which has been shown to lower complication rate and improve overall fracture fixation [7]. However, it is important to note that the PHILOS plate is not specifically designed to address greater tuberosity fractures, potentially resulting in plate-humerus mismatch and postoperative issues like mal-reduction and impingement [8]. Several investigations have explored the use of locking plates in treating greater tuberosity fractures of the humerus. One study examined the biomechanical characteristics of various locking plate designs for these fractures and suggested that plates with a lower profile and shorter span may offer advantages by reducing stress concentration and enhancing fixation stability [9]. Consequently, there remains a need for innovative locking plate designs tailored specifically to the treatment of greater tuberosity (GT) fractures.

Various surgical techniques [10], [11] have been proposed for GT fractures, including suture fixation, screw fixation, tension banding, anchor sutures, and

arthroscopic anchor sutures [12]–[14]. While arthroscopic anchor suture fixation has yielded satisfactory outcomes [15]–[17], it requires a substantial learning curve and may not be suitable for larger or comminuted fragments [17]–[19]. Currently, no universally accepted gold standard exists for treating displaced GT fractures. In contrast, our scepter locking plate design is tailored to match the proximal humeral anatomy and GT region. Compared to traditional locking plates, its shorter length allows for smaller incisions and reduced soft tissue trauma. The low-profile design, adjustable length, and lateral angle mitigate hardware-related issues like impingement. Furthermore, the strategically placed suture holes facilitate secure tension band-type suturing to withstand the physiological load of the rotator cuff on the GT fracture.

The finite element method has gained popularity as a computation technique for analyzing scientific research and industrial applications in many fields, such as solid mechanics, heat transfer, fracture mechanics, fluid dynamics, and biomechanics [20]–[24]. Finite element analysis was used to study biomechanical and elasticity behavior in the locking plate system for proximal humerus fixation [25], [26]. Only one finite element analysis study varied the hole shape of a locking plate [27]. Most finite element analysis studies are based on elasticity. Several design factors were recently studied and proposed in research works [28]. There are several design variables for improved locking plate biomechanical performance, such as the geometric dimensions of plates [29]–[31], plate position [32], [33], screw number [34], screw angle [35], [36], and screw size [37], [38].

This study introduces a new geometric design of a locking plate in a scepter shape. It implements fiber wire to reduce the number of screws, optimized based on the biomechanical performance of the PHILOS plate with suture augmentation to the rotator cuff and evaluated using finite element analysis (FEA) in elasticity. We hypothesize that the new locking plate system will exhibit biomechanical behavior comparable to or non-inferior to the PHILOS plate while being more compact and shorter, as well as 74% lower volume and weight, potentially offering improved surgical techniques and outcomes.

**Table 1:** Material properties in elasticity.

Structure	Modulus of Elasticity (GPa)	Poisson's Ratio	Ref.
Cortical bone of humerus	16	0.3	[39]
PHILOS plate and screw	200	0.265	[40]
Scepter locking plate and screw	200	0.265	[41]
Fiber wire No.5	8.5	0.39	[41]
Supraspinatus tendon	0.168	0.49	[42]
Infraspinatus tendon	0.168	0.49	[42]

## 2 Materials and Methods

### 2.1 Models and material properties

The 3D geometric models of the humerus were determined from a computed tomography (CT) scan of a healthy 24-year-old man and then saved in Digital Imaging and Communications in Medicine (DICOM) format. These images were imported to Mimic 10.1 Software to generate an STL file. Finally, the model was imported to SolidWorks 2018 software to determine the final 3D CAD humerus model. The shape of Supraspinatus and Infraspinatus tendons were reconstructed from an Anatomical study [43] and a previous report [44]. Material properties were assigned for humerus cortical bone, supraspinatus infraspinatus, as shown in Table 1. Cortical bone of humerus was considered to have homogeneous property. Linear elastic analysis was applied in this study. Three-dimensional models of plate and screws were constructed using SolidWorks (Dassault Systemes SolidWorks Corp., Concord, MA, USA) and imported in Abaqus (Dassault Systemes, Waltham MA, USA) to create finite element model and simulate the loading conditions and regions of von Mises stress distribution. The dimensions of the PHILOS plate and screws were taken from the Synthes brochure and previous study [40]. The screws were modeled as smooth cylinders without threads of a diameter of 3.5 mm, according to studies by Mendoza-Muñoz I [45].

A scepter locking plate is a stainless steel 316L reconstruction locking plate at the proximal part and a locking plate at the distal part. It is a low-profile plate with a length of 48.3 mm, width of 23 mm, and thickness of 2.0 mm proximal and distal. This plate has 8 holes for 3.5 mm diameter locking screws with four K-wires and suture holes, as shown in Figure 1(b).

The material properties of stainless steel 316L were assigned according to ASTM standards [40], as shown in Table 2. The GT fracture of the humerus model was established based on the previous study [10], [46]. A split-type GT fracture model as a single large piece based on the study by Pisitwattanaporn *et al.* [46], ensures that the fractured bone segment closely

resembles the fracture depicted in Figure 1, part D, of the study by Zeng *et al.*, [10]. The PHILOS plate with rotator cuff suture with two fiber wires No.5 was drawn according to the study of Pisitwattanaporn *et al.* [46], as shown in Figure 2(a). A scepter locking plate with two fiber wires No.5 was drawn and applied plate at about 1 cm below the tip of the greater tuberosity, and three 3.5 mm cylinder screws were inserted. The Supraspinatus and Infraspinatus were sutured at 1 cm above the greater tuberosity with two fiber wires No.5 and passed the two tails of each suture through the most upper holes of the plate and joined together, as shown in Figure 2(b).

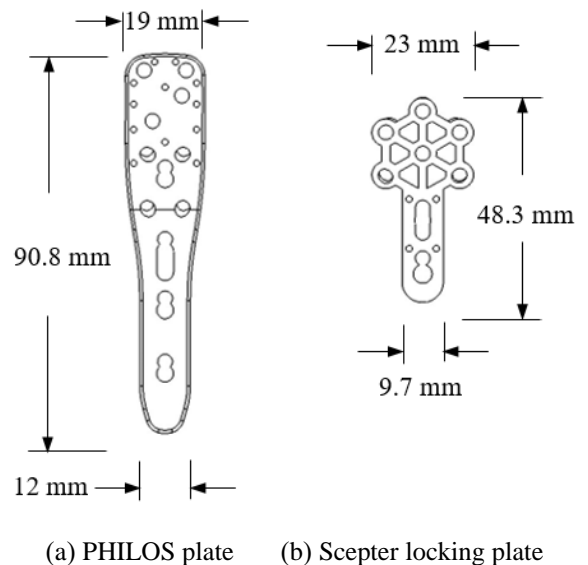


**Figure 1:** Dimensions of PHILOS and scepter plates.

**Table 2:** Material properties of stainless steel 316L.

Material	
Modulus of elasticity (GPa)	200
Shear modulus (GPa)	82
Poisson's ratio	0.265
Mass density (g/cm <sup>3</sup> )	8.027
Yield strength (N/mm <sup>2</sup> )	690

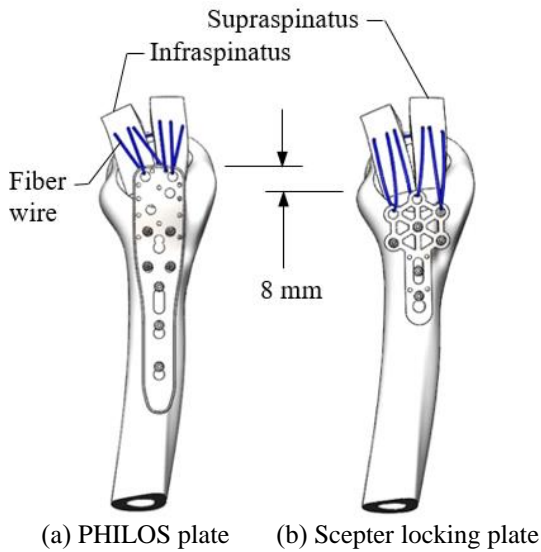


**Figure 2:** Locking plate with Rotator cuff suture with two fiber wires No.5.

Tetrahedral element with 4 nodes/element, C3D4, and hexahedral element with 8 nodes/element, C3D8, were used to construct a finite element model, as shown in Table 3. Mesh independence was applied. Element size was reduced until maximum magnitude, i.e., stress, strain, and displacement were less than 1%. If the element size is extremely small, the computational time is too long without any significant differences in results. The proper size is shown in Table 3. Supraspinatus, infraspinatus, PHILOS plate, scepter plate, bone, and bone crack are defined as an element size of 1 mm. While screws and fiber wires were used 0.25 mm and 0.1 mm, respectively. The finite element models are 430,188 nodes and 1,337,194 elements for the PHILOS plate system and 526,586 nodes and 1,240,018 elements for the scepter plate system. The length of fiber wires in the scepter plate system is 20% longer than in the PHILOS plate system. Then, the total mesh of the scepter plate system is greater than that of the PHILOS plate system.

**Table 3:** Element type and element size.

Part	Element Type	Element Size (mm)
Supraspinatus	C3D4	1
Infraspinatus	C3D4	1
PHILOS plate	C3D4	1
Scepter plate	C3D4	1
Bone	C3D4	1
Crack bone	C3D4	1
Screw	C3D4	0.25
Fiber wire	C3D8	0.1

## 2.2 Boundary condition and external load

The interactions bone-bone, tendon-cartilage, tendon-suture, bone-plate, bone-screw, and screw to the plate were modeled using a frictionless surface-to-surface contact formation and defined a coefficient of friction of 0.1 between surfaces according to the previous study [42] that studied the finite element model for geometrical and mechanical comparison of the three suture positions, i.e., single row, double row, and transosseous with friction coefficient equal to 0.1 between the supraspinatus and bone.

During intense activity, such as various exercises, athletic activities and maximum contraction of supraspinatus produced, the maximum contraction force transmitted highest force through the supraspinatus and infraspinatus tendons were 200 N [47] and 100 N [48], respectively, as well as distributed over medial surface of each tendon. The loading direction was defined as the mean direction of the tendon on the loading surface [49]. A tension force of 10 N was applied to fiber wires. The humerus was fixed at the base to avoid rigid body motion, as shown in Figure 3.

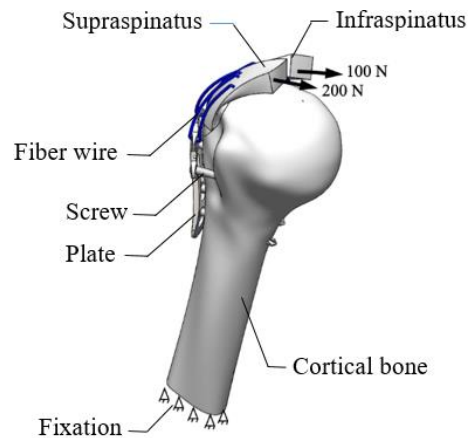


**Figure 3:** Boundary conditions.

## 3 Results and Discussion

### 3.1 Comparisons of maximum von Mises stress of the two fixation models

This paper specifically compared a scepter plate with the PHILOS locking plate because previous studies have established that locking plates provide superior fixation strength for greater tuberosity fractures

compared to alternative methods such as screws and tension band wiring. The PHILOS system was selected as a control because it is widely available and represents the current standard of care for greater tuberosity fracture fixation, as demonstrated in previous research (43). While other locking plate systems exist (10,14,45), they are not yet widely adopted or considered standard treatment options for greater tuberosity fractures.

After applying boundary conditions to a finite element model, the finite element analysis was used to solve the displacement, strain, and stress problems. Figure 4 shows the stress distribution of the PHILOS system model and sceptor locking plate system model. The gray color explains the maximum stress, and stress will be reduced from grey, red, yellow, green, and blue, which is the minimum stress. The meaning of these color contours is also used in all figures. The

maximum stress and a factor of safety of the PHILOS system are 675.2 N/mm<sup>2</sup>, 1.02, respectively, on the head of the screw and sceptor locking plate is 590.9 N/mm<sup>2</sup>, 1.16, respectively, on the plate as shown in Figure 5. It implies that there is no failure on both screw and plate under this load condition. The internal forces acting on the fiber wire in the PHILOS plate and the sceptor locking plate systems were calculated to be 46.88 N and 48.42 N, respectively. Previous studies [41] show that the fiber wire can tolerate a maximum load of  $620 \pm 29$  N before failure. This indicates that the internal forces on the fiber wire in both models are well below the wire's failure threshold, ensuring that the wire remains intact. This study is the first to calculate the forces within the fiber wire in the context of a locking plate system for treating split-type greater tuberosity (GT) avulsion fractures.

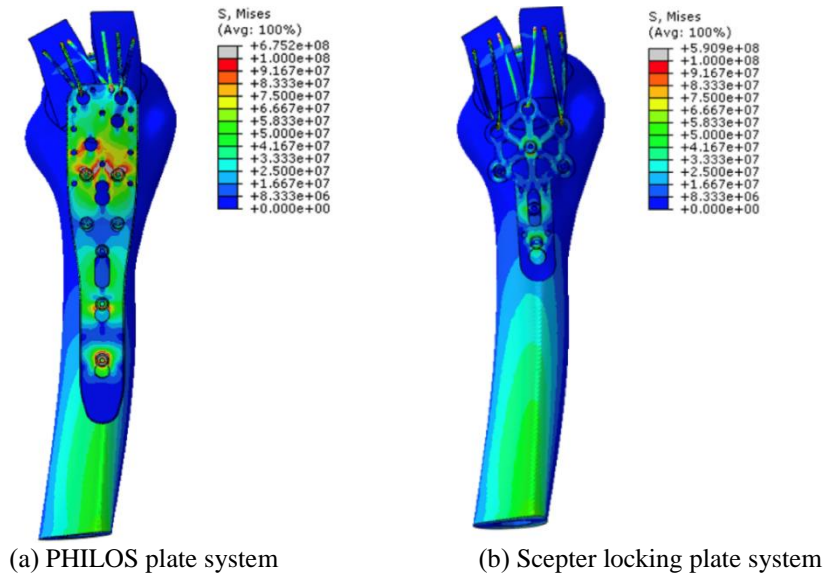


**Figure 4:** Von Mises stress on (a) PHILOS and (b) Sceptor locking plate system.

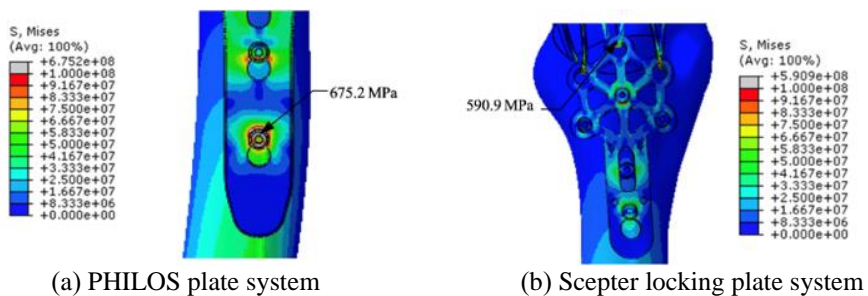


**Figure 5:** The maximum stress concentration of (a) PHILOS and (b) Sceptor locking plate system.

### 3.2 Comparisons of stress on two plates

Figure 6 shows the maximum von Mises stress of 334.1 and 590.9 N/mm<sup>2</sup> on the PHILOS and sceptor locking plates, respectively. The internal force and moment of the lowest screw in the PHILOS model are higher than other screws; then the maximum stress expresses on the lowest hole. For a sceptor model, the

internal force on the fiber wire at the middle top hole is higher than others, and the maximum stress occurs here. The yield strength of plate material is 690 N/mm<sup>2</sup>. This shows that the safety of the PHILOS plate and sceptor locking plate are 2.07 and 1.17, respectively. This implies that both designs can maintain the elasticity behavior or have no failure under specified forces and constraints.

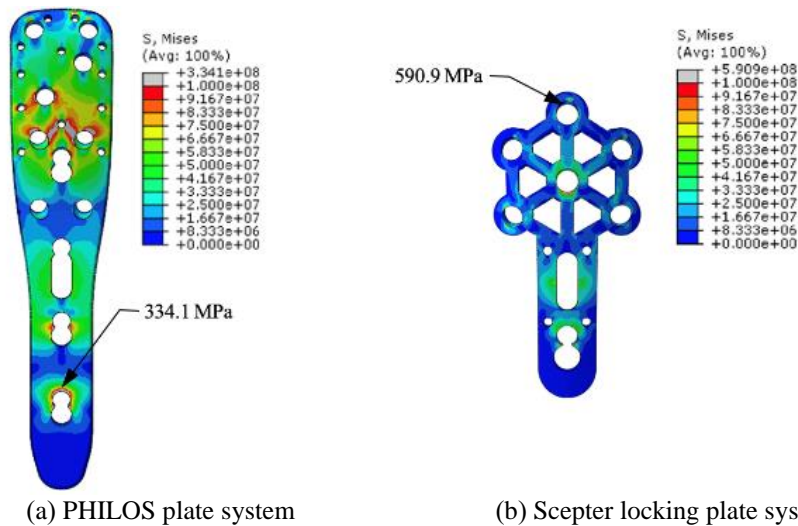


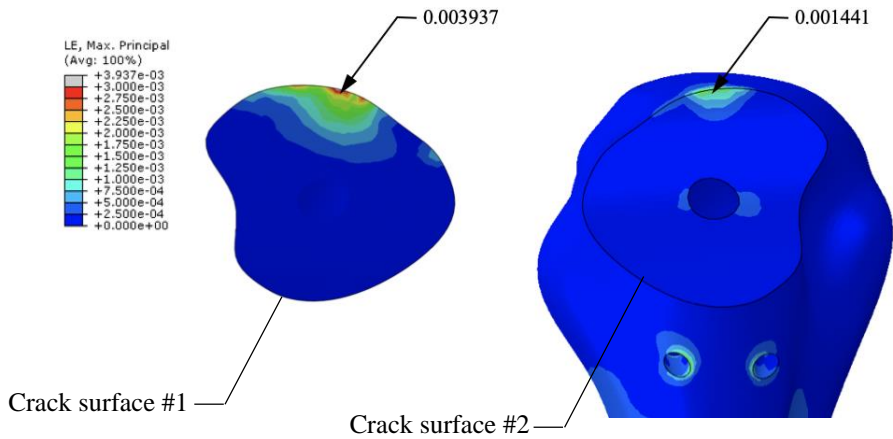
**Figure 6:** The maximum stress concentration of (a) PHILOS and (b) Sceptor locking plate.

Figures 7 and 8 show the maximum strain of two crack surfaces and maximum displacement of fracture gap of the PHILOS system model and sceptor locking plate system model were 0.3937%, 0.54 mm, and 0.492%, 0.49 mm, respectively. The proper strain and maximum displacement of fracture gap that can promote primary healing are less than 2% and 1 mm [50], respectively. The gray color explains the maximum strain, and strain will be reduced from grey, red, yellow, green, and blue color is the minimum strain.

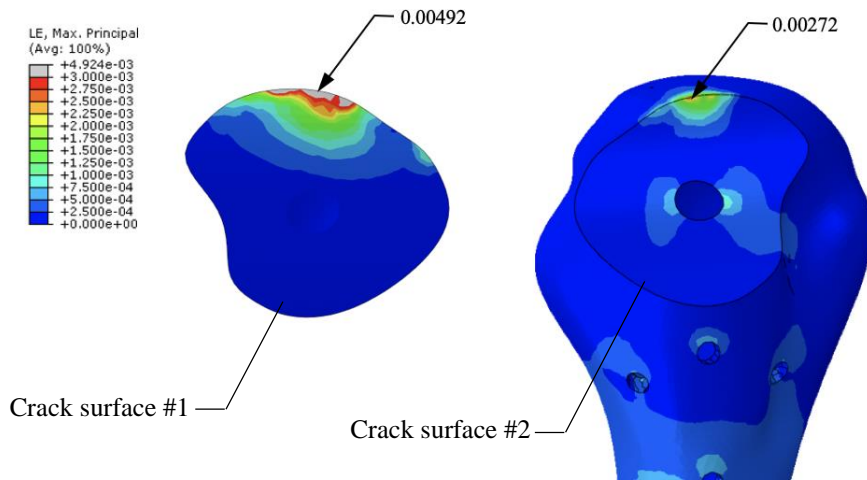
For specification comparison between the sceptor locking plate and the PHILOS plate, the

sceptor locking plate is shorter by 45%, thinner by 20%, and wider by 21% than the PHILOS plate. The volume or weight of the sceptor plate is lower by 74% than the PHILOS plate, as shown in Table 4.

This study demonstrates that the sceptor locking plate system meets the anatomical requirements for treating split-type GT avulsion fractures, performing similarly to the PHILOS plate with rotator cuff suture augmentation. The maximum strain at the fracture site for both plate systems, as shown in Table 5, is less than 2%, and the maximum fracture gap displacement is less than 1 mm [50], facilitating primary bone healing.



(a) The strain concentration of two crack surfaces of PHILOS plate system



(b) The strain concentration of two crack surfaces of the scepter locking plate system

**Figure 7:** The strain concentration of two surfaces of (a) PHILOS and (b) Scepter locking plate system.

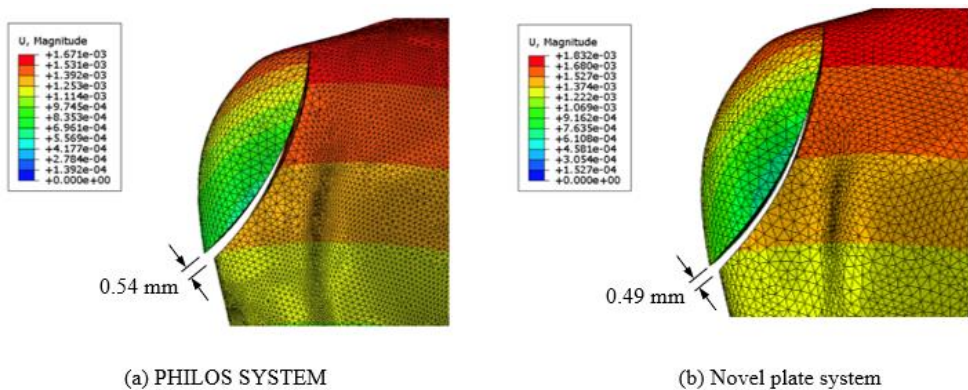


**Figure 8:** The displacement of fracture Gap of (a) PHILOS and (b) Scepter locking plate system.

**Table 4:** Comparison of scepter locking plate and the PHILOS plate.

	Scepter Locking Plate	PHILOS Locking Plate
Length (mm)	48.3	89.4
Width (mm)	23.0	19.0
Thickness (mm)	2.0	2.5
Volume (mm <sup>3</sup> )	820	3,130
Weight (g)	6.58	25.13

At the equilibrium point, the maximum displacement of the fracture gap for the scapular plate is lower than the PHILOS plate, demonstrating better stability in bone fracture fixation. The GT bone fragment movement results in less displacement, as shown in Table 5. The calculated maximum stress values were compared against the material properties.

**Table 5:** Comparison of maximum strain and displacement of fracture gap of both plate systems.

Plate System	Maximum Strain	Displacement of Fracture Gap (mm)
PHILOS	0.003937	0.54
Scepter	0.00492	0.49

Based on the above analysis, both plate types can effectively fix the bone to facilitate fracture healing without plate deformation when calculated at the equilibrium point. However, it is necessary to conduct further trials in real-world environments, including cadaveric testing and actual patient surgeries, to validate the results of this computational study.

From the results of this study, it was found that the maximum stress occurring on the PHILOS plate is at the location of the lowest screw. Additionally, most of the stress is concentrated in the middle portion of the plate, but low stress occurs around the outer edges and lower end, as shown with the blue color contour in Figure 6(a). Furthermore, the suture cord that connects the PHILOS plate to the rotator cuff tendon, which is an important tensile force for the fractured bone, has a limited area for transferring. It implies that the suture cord can handle the transfer force and reduce some screws in the PHILOS system.

The PHILOS plate has a smaller cross-sectional area than the scepter plate. This may result in a poorer distribution of forces across various plate parts. The above information supports the idea that the newly designed locking plate can be made shorter, thinner, and wider. Additionally, when looking at the simulation results, the scepter locking plate design exhibits better stress distribution throughout the plate. The maximum stress at the top portion of the scepter

locking plate still does not exceed the yield point of the material used in this study.

While previous studies have evaluated locking plates for GT fractures [6], [10], [46], including some using FEA [47], [51], these prior works did not account for the impact of rotator cuff suture augmentation in their computational models. Our research represents one of the first efforts to incorporate suture augmentation techniques in the FEA of a scepter locking plate design optimized specifically for GT fractures. By including this crucial factor, which has been shown to improve fracture fixation and lower complication rates [8], our study provides a more comprehensive and clinically relevant evaluation of the proposed implant's biomechanical performance.

Previous studies utilized cadaveric models [45] or compared existing locking plates to other fixation techniques [11], [14] without conducting detailed computational modeling and stress analysis tailored to an optimized implant design considering suture augmentation. By leveraging finite element simulations that account for suture augmentation, our research provides valuable insights into the biomechanical performance of a scepter locking plate meticulously engineered for greater tuberosity fractures, addressing a critical gap in the current literature.

This study provides valuable biomechanical insights, but certain limitations should be acknowledged. The FEA relies on simplified assumptions and literature-based material properties, which may not fully capture the complex behavior of biological tissues and their interactions. In addition, the simulated loading conditions also represent a specific scenario of maximum tendon forces, whereas the shoulder joint experiences a wide range of loading patterns during various activities. Moreover, the study focuses on the immediate post-operative scenario and does not account for the effects of bone healing and tissue remodeling over time. Further investigations, including cadaveric studies and clinical trials, are necessary to validate the findings and evaluate the long-term performance of the scepter locking plate design in vivo.

## 4 Conclusions

In conclusion, the scepter locking plate system presents a viable alternative for treating split-type GT avulsion fractures. This plate system fulfills the

necessary biomechanical requirements for managing isolated split-type GT avulsion fractures. Notably, it is characterized by a low-profile design, shorter length, lower volume and weight compared to standard locking plates, adaptability in lateral angle and length tailored to the humeral bone, and strategically placed holes that allow sutures to be securely tied. Further clinical studies are warranted to confirm the clinical utility of this plate system in the treatment of isolated GT fractures.

### Acknowledgments

This research is supported by Thailand Science Research and Innovation (TSRI) Fundamental Fund fiscal year 2024, Thammasat School of Engineering (TSE), Thammasat University Center of Excellence in Computational Mechanics and Medical Engineering, and Thammasat University.

### Author Contributions

R.W.: conceptualization, data curation, writing—reviewing and editing, project administration. All authors have read and agreed to the published version of the manuscript; P.K: finite element analysis; W.L.: conceptualization, investigation, writing—reviewing and editing.

### Conflicts of Interest

All of the authors declare that they have no conflict of interest.

### References

- [1] C. M. Court-Brown, A. Garg, and M. M. McQueen, “The epidemiology of proximal humeral fractures,” *Acta Orthopaedica Scandinavica*, vol. 72, no. 4, pp. 365–371, 2001.
- [2] C. M. Robinson, A. Akhtar, M. Mitchell, and C. Beavis, “Complex proximal humeral fractures in adults - A systematic review of management,” *Injury*, vol. 42, no. 4, pp. 347–358, 2011.
- [3] F. Brunner, C. Sommer, C. Bahrs, R. Heuwinkel, C. Hafner, P. Rillmann, G. Kohut, A. Ekelund, M. Muller, and L. Audigé, “Open reduction and internal fixation of proximal humerus fractures using a proximal humeral locked plate: A prospective multicenter analysis,” *Journal of Orthopaedic Trauma*, vol. 23, no. 3, pp. 163–172, 2009.
- [4] M. Dominic, W. Markus, G. Boyko, N. Stefaan, and V. Peter, “Computational optimisation of screw orientations for improved locking plate fixation of proximal humerus fractures,” *Journal of Orthopaedic Translation*, vol. 25, pp. 96–104, 2020.
- [5] C. C. Wu, W. J. Chen, C. I. Tai, K. Y. Hsu, P. H. Wang, and C. F. Chen, “Treatment of displaced greater tuberosity fractures of the humerus with locking plates,” *Journal of Trauma*, vol. 68, no. 6, pp. 1411–1416, 2001.
- [6] G. Brais, J. Ménard, J. Mutch, G. Y. Laflamme, Y. Petit, and D. M. Rouleau, “Transosseous braided-tape and double-row fixations are better than tension band for avulsion-type greater tuberosity fractures,” *Shoulder and Elbow*, vol. 12, no. 3, pp. 174–181, 2020.
- [7] D. R. Shukla, S. McAnany, C. Pean, S. Overley, A. Lovy, and B. O. Parsons, “The results of tension band rotator cuff suture fixation of locked plating of displaced proximal humerus fractures,” *Injury*, vol. 48, no. 2, pp. 474–480, 2017.
- [8] H. Kim, Y. G. Chung, J. S. Jang, Y. Kim, S. B. Park, and H. A. Song, “Why locking plates for the proximal humerus do not fit well,” *Archives of Orthopaedic and Trauma Surgery*, vol. 142, no. 2, pp. 219–226, 2022.
- [9] B. Gueorguiev, F. Dyrna, S. Schleifenbaum, O. Pieske, C. A. Müller, L. Löhner, M. Windolf, and M. Knobe, “Biomechanical evaluation of locking plate constructs for the fixation of proximal humerus fractures,” *Injury*, vol. 45, no. 4, pp. 744–749, 2014.
- [10] L. Q. Zeng, Y. F. Chen, Y. W. Jiang, L. L. Zeng, X. G. Miao, and W. G. Liang, “A new low-profile anatomic locking plate for fixation of comminuted, displaced greater tuberosity fractures of the proximal humerus,” *Journal of Shoulder and Elbow Surgery*, vol. 30, no. 6, pp. 1402–1409, 2021.
- [11] D. M. Rouleau, J. Mutch, and G. Y. Laflamme, “Surgical treatment of displaced greater tuberosity fractures of the humerus,” *Journal of the American Academy of Orthopaedic Surgeons*, vol. 24, no. 5, pp. 324–330, 2016.
- [12] Q. Sun, W. Ge, G. Li, J. Z. Wu, G. Lu, and R. Li, “Plate fixation versus arthroscopic-assisted plate fixation for isolated medium-sized fractures of the greater tuberosity: A retrospective study,” *Orthopaedic Surgery*, vol. 10, no. 2, pp. 124–131, 2018.

- [13] D. R. Kim, Y. M. Noh, and S. Y. Lee, "Arthroscopic reduction and suture bridge fixation of a large displaced greater tuberosity fracture of the humerus," *Arthroscopy Techniques*, vol. 8, no. 9, pp. e975–e985, 2019.
- [14] D. Popp, V. Schöffl, and W. Strecker, "Osteosynthesis of displaced fractures of the greater tuberosity with the Bamberg plate," *Der Unfallchirurg*, vol. 112, no. 6, pp. 550–554, 2009.
- [15] P. Platzer, G. Oberleitner, F. Kutscha-Lissberg, T. Wieland, V. Vecsei, and C. Gaebler, "Displaced fractures of the greater tuberosity: A comparison of operative and nonoperative treatment," *Journal of Trauma*, vol. 69, no. 4, pp. 1040–1044, 2010.
- [16] V. Braunstein, W. Plitz, O. J. Muensterer, W. Mutschler, and S. Hinterwimmer, "Operative treatment of greater tuberosity fractures of the humerus - A biomechanical analysis," *Clinical Biomechanics*, vol. 24, no. 8, pp. 675–680, 2009.
- [17] Z. T. Kokkalis, E. Papanikos, E. Bavelou, G. Togias, and S. Sioutis, A. F. Mavrogenis, A. Panagopoulos, "Arthroscopic reduction and fixation of greater tuberosity fractures of the humerus," *European Journal of Orthopaedic Surgery and Traumatology*, vol. 31, no. 6, pp. 1055–1060, 2021.
- [18] W. Liao, H. Zhang, Z. Li, and J. Li, "Is arthroscopic technique superior to open reduction internal fixation in the treatment of isolated displaced greater tuberosity fractures," *Clinical Orthopaedics and Related Research*, vol. 474, no. 5, pp. 1269–1279, 2016.
- [19] S. E. Park, J. J. Jeong, K. Panchal, J. Y. Lee, H. K. Min, and J. H. Ji, "Arthroscopic-assisted plate fixation for displaced large-sized comminuted greater tuberosity fractures of proximal humerus: A novel surgical technique," *Knee Surgery, Sports Traumatology, Arthroscopy*, vol. 24, no. 12, pp. 3892–3898, 2016.
- [20] S. Phongthanapanich and P. Dechaumphai, "Nodeless variable finite element method for stress analysis using flux-based formulation," *Journal of Mechanical Science and Technology*, vol. 22, no. 4, pp. 639–646, 2008.
- [21] P. Soranansri, T. Rojhirunsakool, N. Nithipratheep, C. Ngaouwnthong, K. Boonpradit, C. Treevisootand, W. Srithong, P. Chuchuaiy, and K. Sirivedin, "Hot forging process design and initial billet size optimization for manufacturing of the talar body prosthesis by finite element modeling," *Applied Science and Engineering Progress*, vol. 15, no. 1, pp. 1–10, 2022.
- [22] S. Phongthanapanich, K. Potjananapasiri, and P. Dechaumphai, "J-integral calculation by domain integral technique using adaptive finite element method," *Structural Engineering and Mechanics*, vol. 28, no. 4, pp. 461–477, 2008.
- [23] M. Hearunyakij and S. Phongthanapanich, "An efficient adaptive finite element method based on EBE-PCG iterative solver for LEM analysis," *Structural Engineering and Mechanics*, vol. 83, no. 3, pp. 353–361, 2022.
- [24] P. Soranansri, T. Rojhirunsakool, N. Nithipratheep, C. Ngaouwnthong, K. Boonpradit, C. Treevisootand, W. Srithong, P. Chuchuaiy, and K. Sirivedin, "Hot forging process design and initial billet size optimization for manufacturing of the talar body prosthesis by finite element modeling," *Applied Science and Engineering Progress*, vol. 15, no. 1, pp. 1–10, 2022.
- [25] M. Dominic, B. Satish, O. Georg, F. Jamed, W. Markus, G. Boyko, and V. Peter, "Comparison of optimal screw configurations in two locking plate systems for proximal humerus fixation – a finite element analysis study," *Clinical Biomechanics*, vol. 70, pp. 105097–105105, 2020.
- [26] L. Yang, Z. Ziyang, Q. Ji, S. Qian, Z. Zian, and P. Chengdong, "Finite element analysis and biomechanical study of sandwich fixation in the treatment of elderly proximal humerus fractures," *Frontiers in Bioengineering and Biotechnology*, vol. 10, pp. 1425643–1425652, 2024.
- [27] Y. K. Zhang, H. W. Wei, K. P. Lin, W. C. Chen, C. L. Tsai, and K. J. Lin, "Biomechanical effect of the configuration of screw hole style on locking plate fixation in proximal humerus fracture with a simulated gap: A finite element analysis," *Injury*, vol. 47, no. 6, pp. 1191–1195, 2016.
- [28] Z. Radovan, B. Pawel, and H. S. Emil, "Biomechanical design optimization of proximal humerus locked plates: A review," *Injury*, vol. 55, pp. 111247–111255, 2024.
- [29] L. R. Huff, P. A. Taylor, J. Jani, J. R. Owen, J. S. Wayne, and N. D. Boardman, "Proximal humeral fracture fixation: A biomechanical comparison of two constructs," *Journal of Shoulder and Elbow Surgery*, vol. 22, pp. 129–136, 2013.
- [30] P. E. Saunders, P. Castaneda, R. Walker, and M. D. McKee, "Biomechanical comparison of

- tuberosity-based proximal humeral locking plate compared to standard proximal humeral locking plate in varus cantilever bending,” *Injury*, vol. 53, pp. 3650–3654, 2022.
- [31] R. Walker, P. Castaneda, J. G. Putnam, E. H. Schemitsch, and M. D. McKee, “A biomechanical study of tuberosity-based locked plate fixation compared with standard proximal humeral locking plate fixation for 3-part proximal humeral fractures,” *Journal of Orthopaedic Trauma*, vol. 34, no. 5, pp. 258–263, 2020.
- [32] S. Mehta, M. Chin, J. Sanville, S. Namdari, and M. W. Hast, “Calcar screw position in proximal humerus fracture fixation: Don't miss high!,” *Injury*, vol. 49, no. 3, pp. 624–629, 2018.
- [33] J. Xu, S. Zhan, M. Ling, D. Jiang, H. Hu, and J. Sheng, “How can medial support for proximal humeral fractures be achieved when positioning of regular calcar screws is challenging? Slotting and off-axis fixation strategies,” *Journal of Shoulder and Elbow Surgery*, vol. 31, no. 3, pp. 573–580, 2022.
- [34] H. Kim, M. J. Shin, E. Kholinne, J. Seo, D. Ahn, and J. W. Kim, “How many proximal screws are needed for a stable proximal humerus fracture fixation?,” *Geriatric Orthopaedic Surgery and Rehabilitation*, vol. 12, pp. 1–8, 2021.
- [35] D. Mischler, J. F. Schader, J. Dauwe, L. Tenisch, B. Gueorguiev, and M. Windolf, “Locking plates with computationally enhanced screw trajectories provide superior biomechanical fixation stability of complex proximal humerus fractures,” *Frontiers in Bioengineering and Biotechnology*, vol. 10, pp. 919721–919730, 2022.
- [36] J. F. Schader, D. Mischler, J. Dauwe, R. G. Richards, B. Gueorguiev, and P. Varga, “One size may not fit all: Patient-specific computational optimization of locking plates for improved proximal humerus fracture fixation,” *Journal of Shoulder and Elbow Surgery*, vol. 31, pp. 192–200, 2022.
- [37] J. W. A. Fletcher, M. Windolf, L. Grünwald, R. G. Richards, B. Gueorguiev, and P. Varga, “The influence of screw length on predicted cut-out failures for proximal humeral fracture fixations predicted by finite element simulations,” *Archives of Orthopaedic and Trauma Surgery*, vol. 139, no. 8, pp. 1069–1074, 2019.
- [38] B. Schliemann, N. Risse, A. Frank, M. Müller, P. Michel, and M. J. Raschke, “Screws with larger core diameter and lower thread pitch increase the stability of locked plating in osteoporotic proximal humeral fractures,” *Clinical Biomechanics*, vol. 63, pp. 52–58, 2019.
- [39] P. Clavert, M. Zerah, J. Krier, P. Mille, J. F. Kempf, and J. L. Kahn, “Finite element analysis of the strain distribution in the humeral head tubercles during abduction: Comparison of young and osteoporotic bone,” *Orthopaedics and Traumatology: Surgery and Research*, vol. 97, no. 3, pp. 262–266, 2011.
- [40] F. Hamandi, R. Laughlin, and T. Goswami, “Failure analysis of PHILOS plate construct used for pantalar arthrodesis paper II—screws and FEM simulations,” *Metals*, vol. 8, no. 12, pp. 999–1010, 2018.
- [41] A. A. Qwam, A. Geeslin, J. King, and P. Gustafson, “A finite element model of a surgical knot,” *Journal of Medical Devices*, vol. 11, no. 4, pp. 041009–041015, 2017.
- [42] M. Mantovani, A. Pellegrini, P. Garofalo, and P. Baudi, “A 3D finite element model for geometrical and mechanical comparison of different supraspinatus repair techniques,” *Journal of Shoulder and Elbow Surgery*, vol. 25, no. 4, pp. 557–563, 2016.
- [43] A. S. Curtis, K. M. Burbank, J. J. Tierney, A. D. Scheller, and A. R. Curran, “The insertional footprint of the rotator cuff: An anatomic study,” *Arthroscopy*, vol. 22, no. 6, pp. 524–528, 2006.
- [44] E. A. White, M. R. Skalski, D. B. Patel, and J. S. Gross, A. Tomasian, and N. Heckmann, “Isolated greater tuberosity fractures of the proximal humerus: anatomy, injury patterns, multimodality imaging, and approach to management,” *Emergency Radiology*, vol. 24, no. 2, pp. 117–123, 2017.
- [45] I. Mendoza-Muñoz, A. Gonzalez-Angeles, M. Gil-Samaniego-Ramos, R. L-Avitia, and C. González-Toxqui, “Evaluation of significant effects on locking plates design for a 2-part fracture of the surgical neck of the humerus using finite element and statistical analysis,” *Biomedical Research*, vol. 29, no. 10, pp. 2122–2133, 2018.
- [46] P. Pisitwattanaporn, N. Saengpetch, S. Thamyongkit, T. Wanitchanont, P. Sa-Ngasoongsong, and P. Aroonjarattham, “Additional cuff suture provides mechanical advantage for fixation of split-type greater tuberosity fracture of humerus,” *Injury*, vol. 53, no. 12, pp. 4033–4037, 2022.



- [47] A. Kaisidis, P. G. Pantos, D. Bochlos, and H. Lindner, "Biomechanical analysis of the fixation strength of a novel plate for greater tuberosity fractures," *Journal of Shoulder and Elbow Surgery*, vol. 30, no. 6, pp. 1402–1409, 2021.
- [48] S. S. Burkhart, "A stepwise approach to arthroscopic rotator cuff repair based on biomechanical principles," *Arthroscopy*, vol. 16, no. 3, pp. 82–90, 2000.
- [49] C. Quental, J. Reis, J. Folgado, J. Monteiro, and M. Sarmento, "Comparison of 3 supraspinatus tendon repair techniques - A 3D computational finite element analysis," *Computer Methods in Biomechanics and Biomedical Engineering*, vol. 23, no. 16, pp. 1387–1394, 2020.
- [50] D. S. Elliott, K. J. Newman, D. P. Forward, D. M. Hahn, B. Ollivere, K. Kojima, R. Handley, N. D. Rossiter, J. J. Wixted, R. M. Smith, and C. G. Moran, "A unified theory of bone healing and nonunion: BHN theory," *Bone and Joint Journal*, vol. 98-B, no. 7, pp. 884–891, 2016.
- [51] L. Shen, Z. Wei, W. Qiu-gen, and C. Yunfeng, "Establishment of a three-dimensional finite element model and biomechanical analysis of three different internal fixation methods for humeral greater tuberosity fracture," *International Journal of Clinical and Experimental Medicine*, vol. 11, no. 4, pp. 3245–3254, 2018.